JMEPEG (2018) 27:2338–2344
https://doi.org/10.1007/s11665-018-3342-6

1059-9495/$19.00

The Effect of Titanium Dioxide (TiO_2) Nanoparticles on Hydroxyapatite (HA)/TiO_2 Composite Coating Fabricated by Electrophoretic Deposition (EPD)

M. Amirnejad, A. Afshar, and S. Salehi

(Submitted June 22, 2017; in revised form September 23, 2017; published online April 9, 2018)

Composite coatings of Hydroxyapatite (HA) with ceramics, polymers and metals are used to modify the surface structure of implants. In this research, HA/TiO_2 composite coating was fabricated by electrophoretic deposition (EPD) on 316 stainless steel substrate. HA/TiO_2 composite coatings with 5, 10 and 20 wt.% of TiO_2, deposited at 40 V and 90 s as an optimum condition. The samples coated at this condition led to an adherent, continuous and crack-free coating. The influence of TiO_2 content was studied by performing different characterization methods such as scanning electron microscopy (SEM), energy dispersive x-ray spectroscopy (EDS), corrosion resistance in simulated body fluid (SBF), coating's dissolution rate in physiological solution and bond strength to the substrate. The results showed that the higher amount of TiO_2 in the composite coating led to increase in bond strength of coating to stainless steel substrate from 3 MPa for HA coating to 5.5 MPa for HA-20 wt.% TiO_2 composite coating. In addition, it caused to reduction of corrosion current density of samples in the SBF solution from 18.92 μA/cm^2 for HA coating to 6.35 μA/cm^2 for HA-20 wt.% TiO_2 composite coating.

Keywords 316 stainless steel, composite, electrophoretic, hydroxyapatite, titanium dioxide

1. Introduction

Hydroxyapatite $Ca_{10}(PO_4)_6(OH)_2$ is a bioactive and biocompatible ceramic that have been extensively used in biomedical applications. Due to the similar chemical composition of HA to that of bone tissue, HA implants in the form of ceramic coatings on metallic substrate or ceramic bulks could strongly bond to the bone and promote the formation of bone tissue on their surface. However, the low toughness of the HA makes it inappropriate to be used as load-bearing implants and its application is more limited to low load-bearing porous implants or coating of metallic implants (Ref 1, 2). Therefore, in HA-coated implants, metallic substrate can carry the load, while HA can bond to the surrounding tissue and support the substrate from corrosion attack in contact to the body fluids. HA coatings can provide more stable position of implants in contact to bone and increase the uniform bone ingrowth at the bone-implant interface. Delamination of the ceramic layer from the metal surface, however, can lead to serious problems such as failure of implant (Ref 2).

Various techniques, such as plasma spraying (Ref 3, 4), pulsed laser deposition (Ref 5), sol-gel method (Ref 6, 7), radio frequency magnetron sputtering (Ref 8) and EPD (Ref 9, 10), have been used to produce HA coatings on implants surfaces. Among them, EPD method has many upsides such as the short formation time, simple equipment, no limits of the shape of the substrate and low temperature of process. However, using high calcination temperature as a post-treatment to increase the adhesion of coating to the substrate may cause to decomposition of HA or changing the properties of the substrate. Recently, composite coatings of HA and other materials such as polymers and ceramics [zirconia (Ref 11), silica (Ref 4), bioglass (Ref 9) and TiO_2 (Ref 12)] have been extensively fabricated and evaluated to improve the low strength bonding of pure HA coatings to the metallic substrates. In this study, the composite of HA and TiO_2 was coated by EPD on 316 stainless steel substrate. The effects of introducing TiO_2 nanoparticles to HA coatings on mechanical properties and adhesion of coating to the substrate have been evaluated in the number of researches (Ref 13, 14), but the effect of TiO_2 content on corrosion and dissolution behavior of electrophoretically deposited porous HA coating has been rarely reported. With this in mind, in this study the effect of TiO_2 content on HA coating was investigated. Hydroxyapatite coatings with 0, 5, 10 and 20 wt.% TiO_2 were electrophoretically deposited. The fabricated coatings were characterized by employing SEM equipped with EDS and x-ray diffraction (XRD). Then bonding strength, corrosion behavior and dissolution of coatings in SBF solution were studied.

2. Materials and Methods

Hydroxyapatite powders (0.2-30 μm, Merck, Germany) and different amounts of TiO_2 nanoparticles (0, 5, 10 and 20 wt.%) (21 nm, Degussa P25, Germany) were dispersed in absolute ethanol and in the presence of triethanolamine (TEA, Merck, Germany) as a dispersant (Ref 15). The HA suspensions with different amounts of TiO_2 were dispersed by sonication for 60 min in order to break weak agglomerates. Stirring was

M. Amirnejad and **A. Afshar**, Materials Science and Engineering Department, Sharif University of Technology, Tehran, Iran; **S. Salehi**, Chair of Biomaterials, Faculty of Engineering Science, University of Bayreuth, Bayreuth, Germany. Contact e-mail: m.amirnejad@stu.nit.ac.ir.

continued for 24 h, and later stability of HA suspensions containing different concentration of TEA has been optimized by sedimentation test.

Electrophoretic deposition setup was consisted of a glass cell containing the HA/TiO_2 suspension, 316 stainless steel substrate electrode, a stainless steel counter electrode and a DC power supply. Commercially available 316 stainless steel plates ($50\times20\times2$ mm^3) were used as a cathode. In order to improve the adhesion of the coating to the substrate by mechanical bonding to rough surfaces, prior to EPD, sandblasting was done with 60-micron alumina particles. Distance from the nozzle to the test piece surface of 316 stainless steel substrate electrode and angle between the direction of the abrasive jet and the test piece flat surface were 10 cm and 90°, respectively. The measured arithmetic mean deviation of the profile "Ra" was measured by a surface roughness meter type MAHR (GMBH, Germany) which was equal to 2.67 ± 0.1 μm.

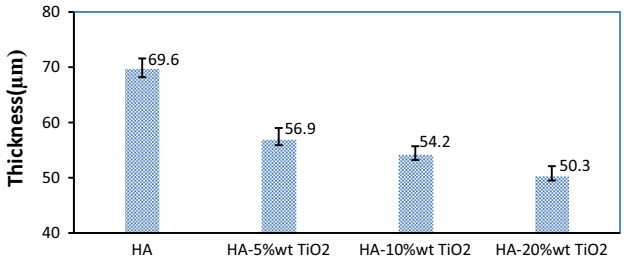

Fig. 1 Thickness of the coatings containing different amount of TiO_2

The separation distance between electrodes in EPD set up was 1.5 cm and constant voltage of 40 V for 90 s was used in EPD process. After coating, samples were dried at room temperature for 24 h and sintered at 500 °C for 2 h under controlled argon atmosphere in order to improve the adhesion of coating to the substrate. Heating and cooling rates were 10 °C/min. Thickness of the coatings was measured using dualscope (MP40 Fischer, Germany) based on the eddy current method.

In order to determine the optimal electrophoretic parameters, deposition was performed at different voltages such as 20, 30, 40 and 60 V for 30, 60, 90, 120 and 150 s from suspension containing 5 wt.% TiO_2.

The surface coating morphologies and their elemental compositions were studied also using scanning electron

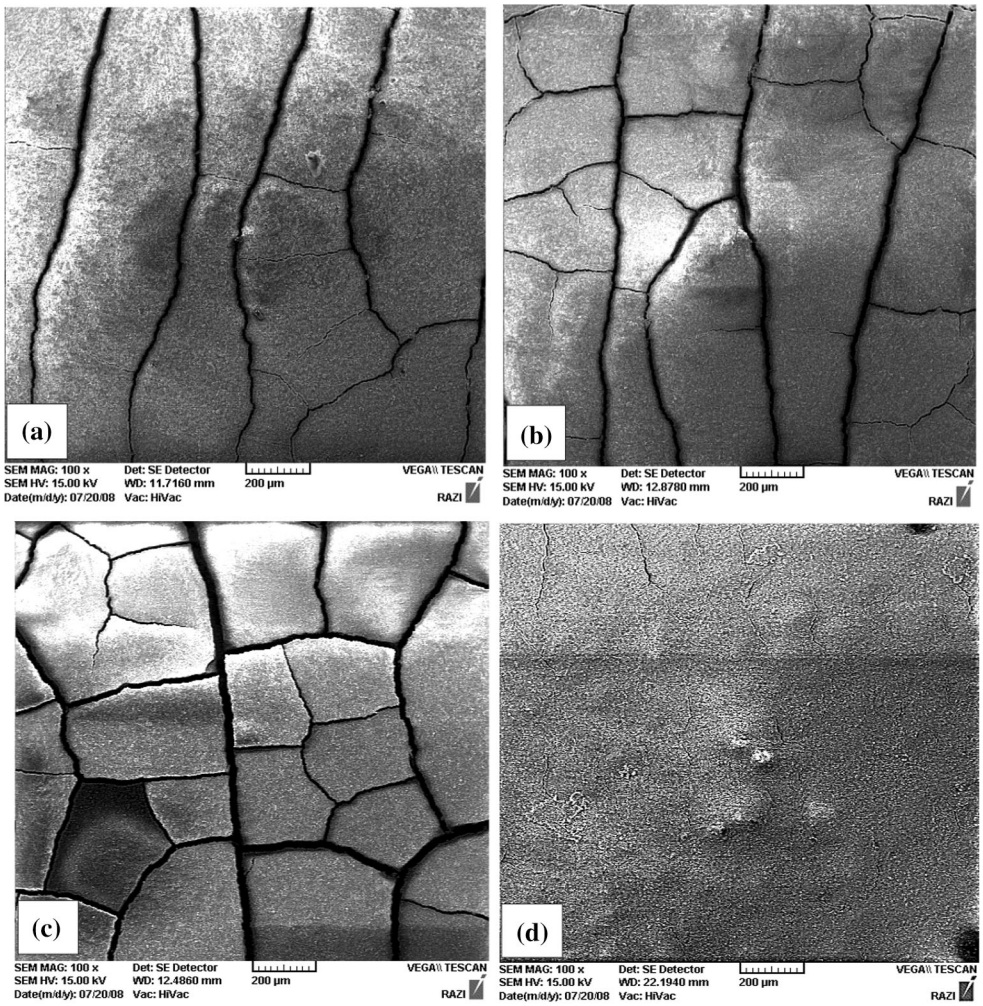

Fig. 2 SEM micrographs of HA-5 wt.% TiO_2 coatings deposited on 316 stainless steel by electrophoretic deposition at (a) 40 V and 120 s (b) 40 V and 150 s (c) 60 V and 90 s (d) 40 V and 90 s after sintering at 500 °C for 2 h

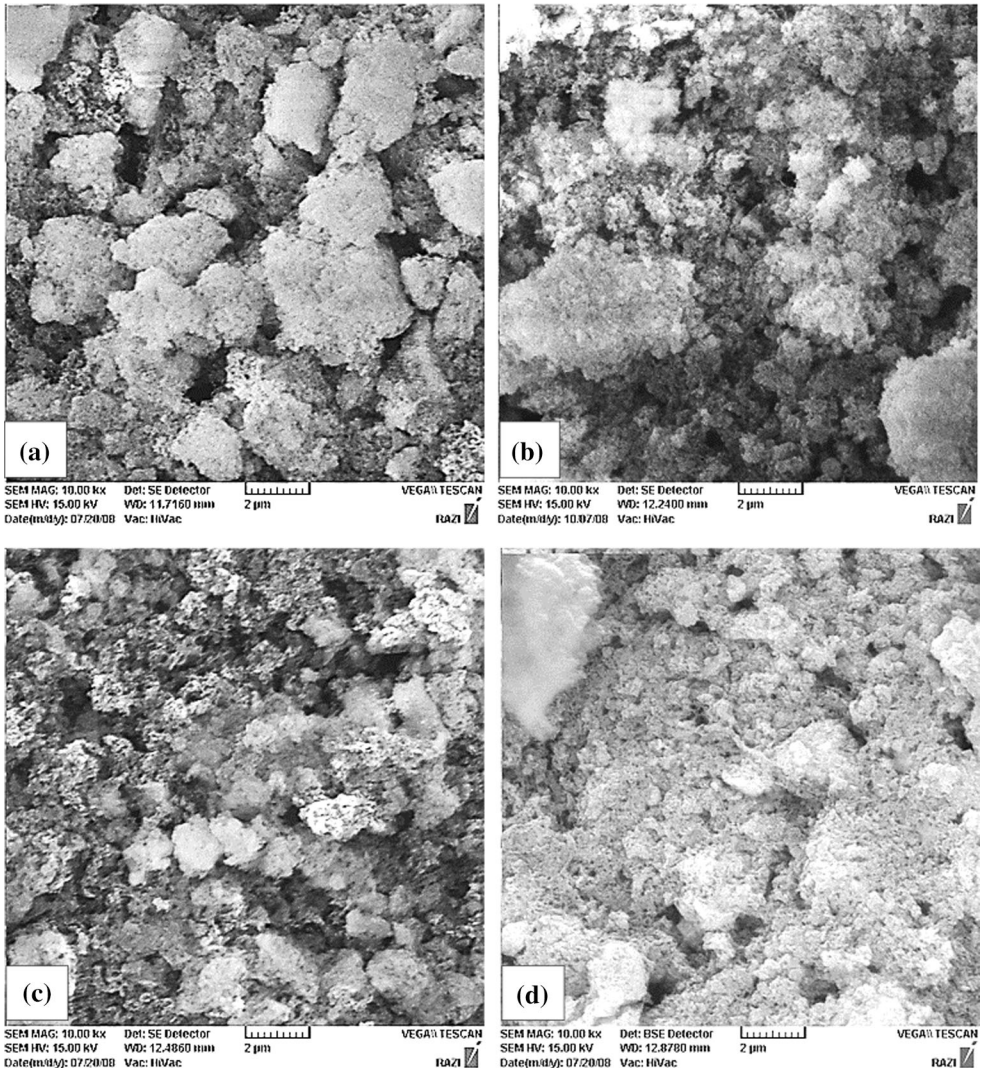

Fig. 3 SEM micrographs of HA and HA/TiO_2 coatings deposited on 316 stainless steel by EPD method at 40 V and 90 s. (a) HA (b) HA-5 wt.% TiO_2 (c) HA-10 wt.% TiO_2 (d) HA-20 wt.% TiO_2

microscopy equipped with energy dispersive x-ray spectroscopy (EDX).

According to Lins et al. (Ref 16), porosity of coating has been investigated by linear polarization method. The polarization resistance is a measure of coating porosity.

The effect of TiO_2 particles on corrosion behavior of coated specimens has been investigated by potentiodynamic polarization test. The electrochemical tests were carried out in SBF solution at 37 °C. Simulated body fluid with an ionic concentration nearly equal to that of human blood plasma was prepared according to the procedure described by Kokubo et al. (Ref 17). A three-electrode cell with a saturate calomel electrode (SCE), a working electrode (the sample) and a counter electrode (platinum plate) was used. The working electrode with an exposed surface area of 1 cm^2 was utilized for all experiments. Polarization curves were obtained by Autolab (EG&G 273A) with a scan rate potential set at 1 mV s^{-1}.

The adhesion strength of the HA coatings containing different amount of TiO_2 was measured by pull off method according to ASTM D4541 (Ref 18). A uniaxial tensile load applied on 25-mm circular coated samples bonded to instrument probe with adhesive bonding glue. The tensile strength was calculated by dividing the load at failure to the cross-sectional area. Five samples were tested for each coated samples with different content of TiO_2.

The crystalline phases of HA/TiO_2 coatings were examined with x-ray powder diffraction (Philips X'Pert-MPD System, Netherlands) using Cu $K\alpha$ radiation (λ = 1.542 Å, 2θ: 20-70°).

The degradation rate of the HA/TiO_2 composite coatings was studied by immersing 1 cm^2 effective surface of the coated samples in a physiological saline solution (0.9% NaCl, pH = 7.42 at 37 °C). The effective coating surface was 1 cm^2 and others covered by lacquer. Solution was replaced every 24 h and analyzed during period of 120 h. After each incubation period, atomic absorption spectroscopy (AAS) was used to measure the Ca^{2+} ions concentration in the solution.

3. Result and Discussion

3.1 Coatings Thickness

Figure 1 shows variation of the thickness of HA and HA/TiO_2 coatings fabricated by EPD method using same deposition

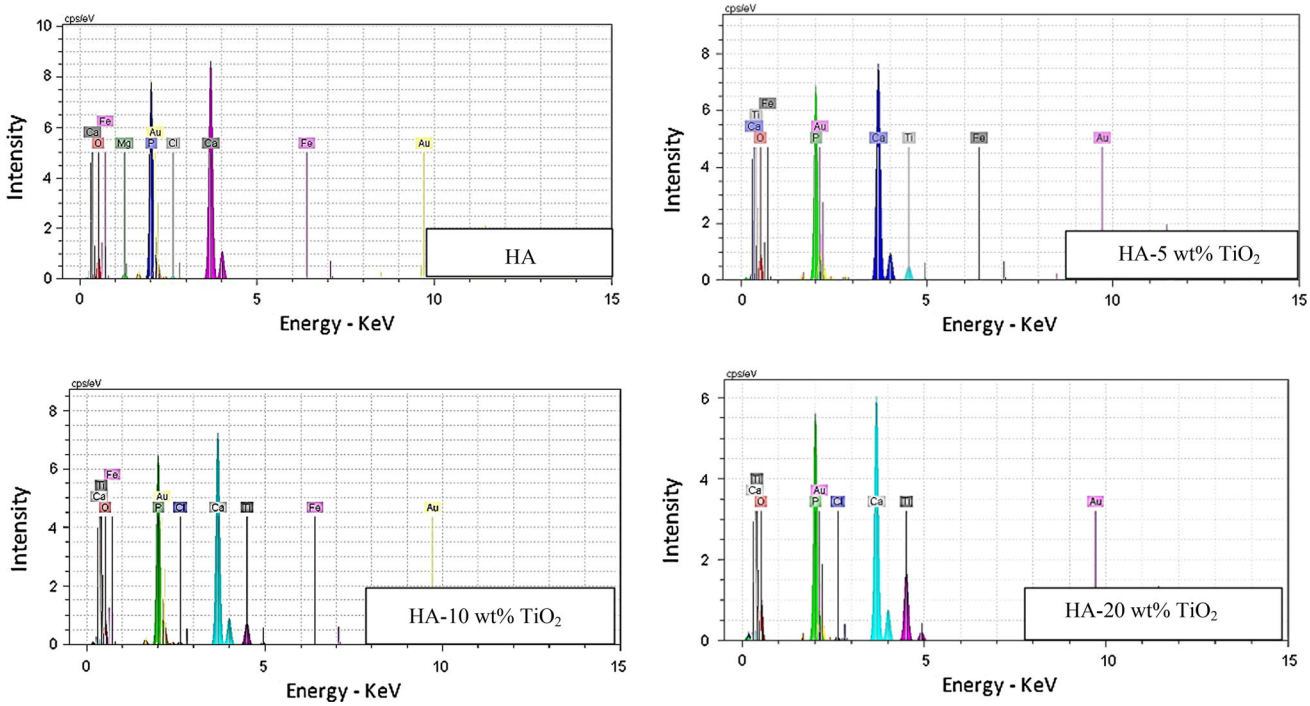

Fig. 4 Chemical compositions of HA and HA/TiO_2 composite coatings containing different amount of TiO_2 analyzed by EDX method

Table 1 The amount of TiO_2 in the suspension and final HA/TiO_2 composite coatings after sintering

TiO_2 in the suspension, wt.%	TiO_2 in the coating, wt.%
5	5.5
10	10.9
20	23.6

Table 2 Polarization resistance of samples

Sample	Polarization resistance, kΩ cm^2
316 SS (bare)	1.37
316 SS with HA coating	1.60
316 SS with HA-5 wt.% TiO_2 coating	1.92
316 SS with HA-10 wt.% TiO_2 coating	2.60
316 SS with HA-20 wt.% TiO_2 coating	4.09

parameters. The results showed reducing trend for the thickness of the coatings by increasing the TiO_2 content in the composition. The main reason is the nanometer size of the TiO_2 particles compared to micrometer size of the HA particles. At a constant voltage, TiO_2 particles in the suspension reduce both the applied electric force on microparticles of HA and their movement into the substrate, resulting in formation of thinner coatings. It should be noted that the optimized thickness of HA coatings on metallic substrates is between 50 and 100 μm thick.

3.2 Coatings Surface Morphology and Chemical Composition

Figure 2 shows the SEM micrographs of coated samples from suspension containing HA and 5 wt.% TiO_2 at various EPD parameters. Results show that EPD at constant voltage of 40 V and 90 s led to uniform, adherent and crack-free coating. Normally during the sintering process, coatings will shrink and crack because of the densification and thermal stresses which are originated from differences in thermal expansion coefficients between ceramic coating and metallic substrate. In this study we arrived to optimize the coating and sintering process to fabricate HA/TiO_2 coatings based on two properties (morphology and thickness). At first we aimed to choose a crack-free and homogenous coating by evaluating their morphology, and at second we measured the thickness of the coatings. According to Yaszemski et al. (Ref 19) coatings with thickness greater than 80 μm become brittle, while very thin HA (less than 50 μm) coatings may resorb too fast and cannot provide the corrosion protection of metallic substrate.

Figure 3 shows the SEM micrographs of HA and HA/TiO_2 composite coatings after sintering at 500 °C for 2 h. The HA coating (Fig. 3a) was not densely packed, and some agglomerated HA particles were present in the coating that made a more porous structure. After increasing the amount of TiO_2 in the coating, the denser and less porous structure comparing to pure HA was formed (Fig. 3b-d)

The elemental compositions of the coatings containing different amount of TiO_2 were studied by EDX analysis, as shown in Fig. 4.

As can be seen in Fig. 4, the main elements in the coatings are Ca and P as well as Ti and O. It proved that the elemental components of the using suspension in EPD method were incorporated into the films. Following the increase in the TiO_2 content in the suspension, the amount of Ti also raised up. We also quantitatively measured the amount of TiO_2 present in the coatings and compared them with the theoretic value in the starting suspension in EPD method. According to Table 1, there

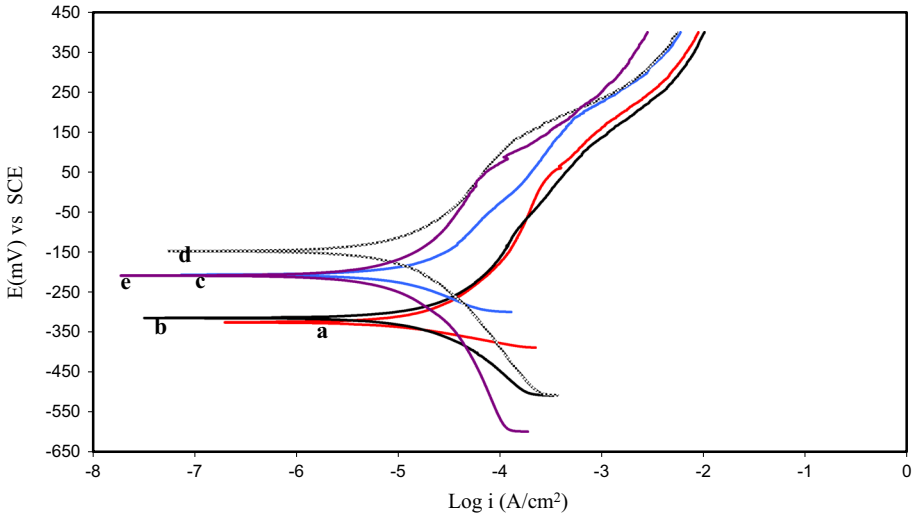

Fig. 5 Potentiodynamic polarization curves of (a) uncoated, (b) HA, (c) HA-5 wt.% TiO_2, (d) HA-10 wt.% TiO_2 and (e) HA-20 wt.% TiO_2 coated 316 stainless steel in SBF solution

Table 3 Values of corrosion current densities and corrosion potentials in SBF solution at 37 °C

Sample	E_{corr}, mV SCE	I_{corr}, μA/cm^2
316 SS (bare)	− 324	18.92
316 SS with HA coating	− 313	16.25
316 SS with HA-5 wt.% TiO_2 coating	− 205	13.40
316 SS with HA-10 wt.% TiO_2 coating	− 146	9.98
316 SS with HA-20 wt.% TiO_2 coating	− 207	6.35

Table 4 The adhesion strength of coatings containing different amount of TiO_2

Coating	Adhesion strength, MPa with standard deviation
HA	3 ± 0.25
HA—5 wt.% TiO_2	3.5 ± 0.3
HA—10 wt.% TiO_2	4.5 ± 0.25
HA—20 wt.% TiO_2	5.5 ± 0.35

is a significant agreement between the calculated amount of TiO_2 in the composite coatings and that of related suspension used in EPD method.

3.3 Corrosion Behavior

Table 2 shows the polarization resistance of uncoated, HA-coated and composite-coated 316 SS measured by linear polarization method.

According to Table 2, uncoated stainless steel has the lowest polarization resistance (Rp = 1.37 kΩ cm^2). HA coating led to increase in polarization resistance to Rp = 1.60 kΩ cm^2. Higher amount of TiO_2 in the coatings results in the increase in the polarization resistance of coatings, and it shows that the presence of TiO_2 in the coating led to less porous coatings. The fact that addition of TiO_2 decreased the porosity in the HA coating was also supported by the SEM examinations (Fig. 3).

The potentiodynamic polarization curves of uncoated, HA-coated and composite-coated 316 SS are shown in Fig. 5. Electrochemical measurements indicated that the composite coatings could protect the stainless steel substrate from corrosion in SBF solution.

The corrosion current densities of different samples were measured from the potentiodynamic polarization curves by linear polarization method. These results align with corrosion potentials are summarized in Table 3.

According to Table 3 and Fig. 5, the uncoated 316 SS substrate possesses lower corrosion resistance and thus higher corrosion current density (i_{corr} = 18.92 μA/cm^2). After coating the substrate by HA the corrosion current density got decreased (i_{corr} = 16.25 μA/cm^2), but this effect is not adequately complete. This was due to the porous structure of HA coating and presence of microcracks in the structure that could not protect the stainless steel substrate in SBF solution. However, HA/TiO_2 composite coatings exhibited a better electrochemical behavior than the pure HA coatings possibly due to the less porosity and the higher density of the coatings. Therefore, crack-free and densely packed coatings formed after increasing the TiO_2 amount in the coating showed higher corrosion resistant comparing to HA coating.

3.4 Adhesion

The adhesion strength of coatings to the metallic substrate was measured using the pull off test, and results are summarized in Table 4. The small increase in adhesion strength was seen after increasing the amount of TiO_2 in the composition.

According to surface morphology of coatings, the HA coating prepared by EPD method showed the porous structure and adding TiO_2 nanoparticles resulted in less porosity of the composite coatings. The less porosity and higher density of

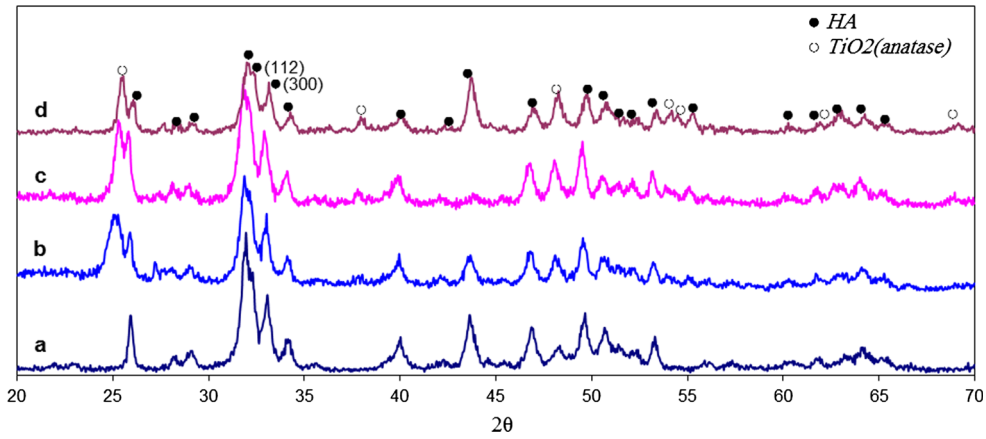

Fig. 6 XRD patterns of composite coatings after sintering at 500 °C for 2 h: (a) HA, (b) HA-5 wt.% TiO_2 (c) HA-10 wt.% TiO_2 (d) HA-20 wt.% TiO_2

Table 5 Calculated crystallinity of HA in the coatings with different amount of TiO_2

Coating	I_{300}	$V_{300/112}$	Crystallinity, %
HA	304.24	121.68	60
HA—5 wt.% TiO_2	310.11	133.35	57
HA—10 wt.% TiO_2	325.84	156.39	52
HA—20 wt.% TiO_2	210.24	105.11	50

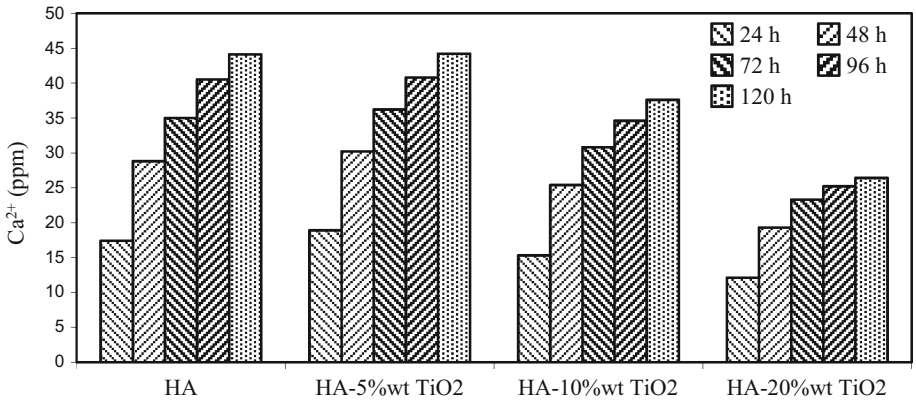

Fig. 7 The concentration of released calcium ions over immersion time in the saline solution

coating lead to higher cohesive strength of the coatings. The improved cohesive strength of the HA/TiO_2 composite coatings resulted in improved bonding between the coating and the substrate. Homogenous distribution of TiO_2 nanoparticles into the porosities of HA structure resulted in increase in adhesion strength. The second strengthening mechanism is uniform distribution of titanium dioxide nanoparticles in the hydroxyapatite coating, called dispersion strengthening phenomena (Ref 13).

3.5 Crystallinity

Figure 6 shows the XRD patterns of composite coatings of HA/TiO_2 after sintering at 500 °C for 2 h.

The patterns show the standard peaks of HA and TiO_2 structure, and there is no sign of decomposition in the HA structure confirming the stability of HA structure after sintering at 500 °C. The crystallinity was calculated using XRD patterns and Pang and Bao et al. equation (Ref 20). The fraction of crystalline phase (X_c) in the HA powders was calculated by the following equation:

$$X_c = 1 - \left(V_{112/300}/I_{300}\right)$$

where I_{300} is the intensity of (300) diffraction peak and $V_{112/300}$ is the intensity of the valley between (112) and (300) diffraction peaks of HA. Table 5 shows the calculated crystallinity of HA in the various coatings.

Results indicated that the presence of TiO_2 in the coatings leads to reduction in HA crystallinity after sintering. It seems that TiO_2 protected the crystalline structure of HA to change to amorphous phase over sintering.

3.6 Dissolution

Figure 7 presents the dissolution behavior of the coatings as a function of immersion time in a physiological saline solution.

The increase in released calcium ions concentrations with increasing amount of TiO_2 up to 5 wt.% in each immersion period is in agreement with decrease in coating crystallinity as a result of TiO_2 presence (see Table 5). It is important to note that amorphous HA is more soluble than crystalline one (Ref 21). In contrast, for each immersion period, the calcium concentration in the solution was lower for HA-10 wt.% TiO_2 and HA-20 wt.% TiO_2 coatings compared with HA and HA-5 wt.% TiO_2. This phenomenon was probably because of the porosity effect on HA dissolution. The lower porosity can decrease the exposed surface of HA particles to the saline solution and decreased dissolution rate of HA respectively.

It can be seen, for all of the coatings, the dissolution occurred quite rapidly. Even though there was rapid dissolution after a short period of time, the dissolution rate decreased with increasing time. The higher dissolution rate can be due to faster solubility of amorphous HA while after decreasing the amount of amorphous phase in the coating the dissolution rate got reduced.

4. Conclusion

Composite coatings of HA/TiO_2 containing different amount of TiO_2 were fabricated by electrophoretic deposition method. The morphology of the composite coatings was continuous and uniform, and the structure was crack-free after sintering at 500 °C for 2 h. The higher amount of TiO_2 in the structure resulted in less porous structure. It could also help to improve the bonding strength of coatings to the substrate from 3 MPa for HA coating to 5.5 MPa for HA-20 wt.% TiO_2 composite coating, and increasing corrosion resistance of coated implant is SBF solution so that corrosion current density decreases from 18.92 μA/cm^2 for HA coating to 6.35 μA/cm^2 for HA-20 wt.% TiO_2 composite coating.

References

1. J.B. Park and J.D. Bronzino, *Biomaterials: Principles and Applications*, CRC Press, Boca Raton, 2002, https://doi.org/10.1007/s13398-014-0173-7.2
2. K.C. Dee, D.A. Puleo, and R. Bizios, *An Introduction to Tissue-Biomaterial Interactions*, Wiley, New York, 2003
3. H. Xu, X. Geng, G. Liu, J. Xiao, D. Li, Y. Zhang, P. Zhu, and C. Zhang, Deposition, Nanostructure and Phase Composition of Suspension Plasma-Sprayed Hydroxyapatite Coatings, *Ceram. Int.*, 2016, **42**, p 8684–8690. https://doi.org/10.1016/j.ceramint.2016.02.102
4. E.S. Bogya, Z. Károly, and R. Barabás, Atmospheric Plasma Sprayed Silica-Hydroxyapatite Coatings on Magnesium Alloy Substrates, *Ceram. Int.*, 2015, **41**, p 6005–6012. https://doi.org/10.1016/j.ceramint.2015.01.041
5. P. Rajesh, N. Mohan, Y. Yokogawa, and H. Varma, Pulsed Laser Deposition of Hydroxyapatite on Nanostructured Titanium Towards Drug Eluting Implants, *Mater. Sci. Eng. C*, 2013, **33**, p 2899–2904. https://doi.org/10.1016/j.msec.2013.03.013
6. D. Sidane, D. Chicot, S. Yala, S. Ziani, H. Khireddine, A. Iost, and X. Decoopman, Study of the Mechanical Behavior and Corrosion Resistance of Hydroxyapatite Sol-Gel Thin Coatings on 316 L Stainless Steel Pre-coated with Titania Film, *Thin Solid Films*, 2015, **593**, p 71–80. https://doi.org/10.1016/j.tsf.2015.09.037
7. S. Ramesh, A.N. Natasha, C.Y. Tan, L.T. Bang, A. Niakan, J. Purbolaksono, H. Chandran, C.Y. Ching, S. Ramesh, and W.D. Teng, Characteristics and Properties of Hydoxyapatite Derived by Sol-Gel and Wet Chemical Precipitation Methods, *Ceram. Int.*, 2015, https://doi.org/10.1016/j.ceramint.2015.04.105
8. M.A. Surmeneva and R.A. Surmenev, Microstructure Characterization and Corrosion Behaviour of a Nano-hydroxyapatite Coating Deposited on AZ31 Magnesium Alloy Using Radio Frequency Magnetron Sputtering, *Vacuum.*, 2015, **117**, p 60–62. https://doi.org/10.1016/j.vacuum.2015.04.004
9. A. Molaei, M. Yari, and M.R. Afshar, Modification of Electrophoretic Deposition of Chitosan-Bioactive Glass-Hydroxyapatite Nanocomposite Coatings for Orthopedic Applications by Changing Voltage and Deposition Time, *Ceram. Int.*, 2015, **41**, p 14537–14544. https://doi.org/10.1016/j.ceramint.2015.07.170
10. A. Tahmasbi Rad, M. Solati-Hashjin, N.A.A. Osman, and S. Faghihi, Improved Bio-Physical Performance of Hydroxyapatite Coatings Obtained by Electrophoretic Deposition at Dynamic Voltage, *Ceram. Int.*, 2014, **40**, p 12681–12691. https://doi.org/10.1016/j.ceramint.2014.04.116
11. Y. Huang, Y. Yan, and X. Pang, Electrolytic Deposition of Fluorine-Doped Hydroxyapatite/ZrO_2 Films on Titanium for Biomedical Applications, *Ceram. Int.*, 2013, **39**, p 245–253. https://doi.org/10.1016/j.ceramint.2012.06.017
12. H. Te Chen, H.Y. Shu, C.J. Chung, and J.L. He, Assessment of Bone Morphogenic Protein and Hydroxyapatite-Titanium Dioxide Composites for Bone Implant Materials, *Surf. Coat. Technol.*, 2015, **276**, p 168–174. https://doi.org/10.1016/j.surfcoat.2015.06.056
13. X.F. Xiao, R.F. Liu, and Y.Z. Zheng, Characterization of Hydroxyapatite/Titania Composite Coatings Codeposited by a Hydrothermal-Electrochemical Method on Titanium, *Surf. Coat. Technol.*, 2006, **200**, p 4406–4413. https://doi.org/10.1016/j.surfcoat.2005.02.205
14. A. Kobayashi and W. Jiang, *Properties of Titania/Hydroxyapatite Nanostructured Coating Produced by Gas Tunnel Type Plasma Spraying*, 2009, **83**, p 86–91. https://doi.org/10.1016/j.vacuum.2008.03.070
15. X.F. Xiao and R.F. Liu, Effect of Suspension Stability on Electrophoretic Deposition of Hydroxyapatite Coatings, *Mater. Lett.*, 2006, **60**, p 2627–2632. https://doi.org/10.1016/j.matlet.2006.01.048
16. V.F.C. de Lins, G.F. de Andrade Reis, C.R. de Araujo, T. Matencio, V. De Freitas, C. Lins, G. Francisco, D.A. Reis, C. Roberto, D. Araujo, and T. Matencio, Electrochemical Impedance Spectroscopy and Linear Polarization Applied to Evaluation of Porosity of Phosphate Conversion Coatings on Electrogalvanized Steels, *Appl. Surf. Sci.*, 2006, **253**, p 2875–2884. https://doi.org/10.1016/j.apsusc.2006.06.030
17. T. Kokubo and H. Takadama, How Useful is SBF in Predicting in Vivo Bone Bioactivity?, *Biomaterials*, 2006, **27**, p 2907–2915. https://doi.org/10.1016/j.biomaterials.2006.01.017
18. ASTM, ASTM D4541-09, Standard Test Method for Pull-Off Strength of Coatings Using Portable Adhesion, *ASTM Int.*, 2014, https://doi.org/10.1520/d4541-09e01.2
19. M. Yaszemski and D.J. Trantolo, *Biomaterials in Orthopedics*, CRC Press, Boca Raton, 2003
20. Y.X. Pang and X. Bao, Influence of Temperature, Ripening Time and Calcination on the Morphology and Crystallinity of Hydroxyapatite Nanoparticles, *J. Eur. Ceram. Soc.*, 2003, **23**, p 1697–1704. https://doi.org/10.1016/s0955-2219(02)00413-2
21. B.D. Ratner, A.S. Hoffman, F.J. Schoen, and J.E. Lemons, *Biomaterials Science: An Introduction to Materials in Medicine*, Academic Press, Amsterdam, 2004